Randomly Punctured LDPC Codes

Mitchell, David G.M.; Lentmaier, Michael; Pusane, Ali E.; Costello Jr., Daniel J.

Published in:
IEEE Journal on Selected Areas in Communications

DOI:
10.1109/JSAC.2015.2507758

2016

Randomly Punctured LDPC Codes

David G. M. Mitchell, *Member, IEEE,* Michael Lentmaier, *Senior Member, IEEE,* Ali E. Pusane, *Member, IEEE,* and Daniel J. Costello, Jr., *Life Fellow, IEEE*

***Abstract*—In this paper, we present a random puncturing analysis of low-density parity-check (LDPC) code ensembles. We derive a simple analytic expression for the iterative belief propagation (BP) decoding threshold of a randomly punctured LDPC code ensemble on the binary erasure channel (BEC) and show that, with respect to the BP threshold, the strength and suitability of an LDPC code ensemble for random puncturing is completely determined by a single constant that depends only on the rate and the BP threshold of the mother code ensemble. We then provide an efficient way to accurately predict BP thresholds of randomly punctured LDPC code ensembles on the binary-input additive white Gaussian noise channel (BI-AWGNC), given only the BP threshold of the mother code ensemble on the BEC and the design rate, and we show how the prediction can be improved with knowledge of the BI-AWGNC threshold. We also perform an asymptotic minimum distance analysis of randomly punctured code ensembles and present simulation results that confirm the robust decoding performance promised by the asymptotic results. Protograph-based LDPC block code and spatially coupled LDPC code ensembles are used throughout as examples to demonstrate the results.**

***Index Terms*—Low-density parity-check (LDPC) codes, spatially coupled codes, rate-compatible codes, punctured codes, iterative decoding, belief propagation, decoding thresholds, binary erasure channel, additive white Gaussian noise channel, minimum distance.**

I. Introduction

IT is often desirable in applications that experience changing channel conditions to be able to employ a variety of code rates. Coding schemes that can adapt to the changing conditions of time-varying channels while allowing transceivers to employ the same encoder/decoder pair are known as *rate-compatible codes* [1]. Rate-compatible low-density parity-check (LDPC) codes have been extensively studied in the literature using code modifying techniques such as information nulling or shortening [2], extending [3]-[6], puncturing [7]-[14], and combining [15].

In a rate-compatible puncturing scheme [1], the transmitter punctures coded symbols and, as a result of having fewer transmitted code symbols, the code rate is increased. It is assumed that the receiver knows the positions of the punctured symbols, so that both the punctured and transmitted symbols can be estimated during decoding. Since the decoder for the mother code is used to decode the punctured codes, a variety of code rates can be achieved using the same decoding architecture by puncturing different numbers of symbols.

In this paper, we consider punctured LDPC codes, where the punctured bits are selected randomly and uniformly over the complete codeword. We derive a simple analytic expression for the iterative belief propagation (BP) decoding threshold of a randomly punctured LDPC code ensemble on the binary erasure channel (BEC) and show that, with respect to the BP decoding threshold, the strength and suitability of an LDPC code ensemble for random puncturing over the BEC is completely determined by a single constant $\theta \geq 1$ that depends only on the rate and BP threshold of the mother code ensemble. If $\theta = 1$, the punctured ensembles are capacity achieving for all higher rates, and if θ is close to 1, the punctured ensemble thresholds are close to capacity for all higher rates up to $1/\theta$.

We extend the BEC results to the binary-input additive white Gaussian noise channel (BI-AWGNC) and show that analogous results can be obtained. In particular, we develop a relationship between the BP thresholds on the two channels and provide an efficient way to predict the thresholds of punctured LDPC code ensembles on the BI-AWGNC given only the BP threshold of the mother code ensemble on the BEC and the code design rate, and we show how the prediction can be improved with knowledge of the BI-AWGNC threshold. The predicted thresholds are shown to be accurate by comparing them with values calculated by discretized density evolution for a variety of code ensembles and puncturing fractions. Throughout the paper, we use protograph-based LDPC block code (LDPC-BC) [16], [17] and spatially coupled LDPC (SC-LDPC) code [18] ensembles, although the approach is valid for general LDPC-BC and SC-LDPC code ensembles. We also perform an asymptotic minimum distance analysis and show that, for asymptotically good LDPC-BC and SC-LDPC mother code ensembles, the randomly punctured code ensembles are also asymptotically good. Moreover, we show that, even though the minimum distance growth rates decrease as the puncturing fraction increases, the gap to the Gilbert-Varshamov bound actually decreases with puncturing. Finally, computer simulations are used to confirm the robust decoding performance promised by the asymptotic results.

The paper provides a unified and comprehensive study of random puncturing of LDPC code ensembles, extending the BEC analysis of [19] and an introductory numerical study for the BI-AWGNC [20]. Compared to [19] and [20], we consider

This work was supported in part by the NSF under Grant Number CCF-1161754 and in part by TUBITAK under Grant Number 111E276. The material in this paper was presented in part at the International Symposium on Turbo Codes and Iterative Information Processing, Bremen, Germany, August 2014 and in part at the IEEE International Symposium on Information Theory, Hong Kong, China, July 2015.

D. G. M. Mitchell is with the Klipsch School of Electrical and Computer Engineering, New Mexico State University, Las Cruces, NM 88003, USA. He was with the Department of Electrical Engineering, University of Notre Dame, Notre Dame, IN 46556, USA (e-mail: dgmm@nmsu.edu).

M. Lentmaier is with the Department of Electrical and Information Technology, Lund University, Lund, Sweden (e-mail: Michael.Lentmaier@eit.lth.se).

A. E. Pusane is with the Department of Electrical and Electronics Engineering, Bogazici University, Istanbul, Turkey (e-mail: ali.pusane@boun.edu.tr).

D. J. Costello, Jr. is with the Department of Electrical Engineering, University of Notre Dame, Notre Dame, IN 46556, USA (e-mail: costello.2@nd.edu).

(J, K)-regular LDPC-BC and SC-LDPC code ensembles of varying densities and rates as well as irregular code ensembles. We also provide an analytical expression for the BP decoding threshold of an arbitrary randomly punctured LDPC code ensemble on the BEC and show that this result is, in fact, independent of the decoding algorithm or the structure of the mother code. For example, we show that a similar argument can be made for the threshold of the maximum a posteriori probability (MAP) decoder. In this case, the derivation is the same and simply leads to a different θ. We further show that, even though the single BEC constant θ can be used to approximate thresholds on the BI-AWGNC, the approximation can be improved by combining the BEC constant and a BI-AWGNC constant, providing an accurate prediction of thresholds for all achievable rates.

The paper is structured as follows: In Section II, we describe the construction of protograph-based LDPC-BC and SC-LDPC code ensembles. In Section III we present an analysis of the thresholds of randomly punctured LDPC code ensembles on the BEC, and in Section IV we extend the analysis to the BI-AWGNC. In Section V, we perform an asymptotic minimum distance analysis of punctured LDPC code ensembles, and computer simulation results are presented in Section VI. Conclusions are provided in Section VII. We remark that the purpose of this paper is to provide a comprehensive analysis of randomly punctured LDPC codes, not to compare various rate-compatible code constructions or to propose optimal puncturing patterns.

II. Background: Protograph-based LDPC Codes

In this section, we describe the LDPC code ensembles used throughout the paper. We choose to consider LDPC codes based on a *protograph* [16] to demonstrate our results, since they have been shown in the literature to have many desirable qualities, such as fast encoding/decoding, low iterative decoding thresholds, and linear minimum distance growth (see, for example, [17], and the references therein).

A. Protograph-based LDPC-BCs

A protograph [16] with *design rate* $R = 1 - n_c/n_v$ is a small bipartite graph that connects a set of n_v variable nodes to a set of n_c check nodes by a set of edges. The protograph can be represented by a parity-check or *base* biadjacency *matrix* $\mathbf{B}$, where $B_{x,y}$ is taken to be the number of edges connecting variable node v_y to check node c_x. The parity-check matrix $\mathbf{H}$ of a protograph-based LDPC-BC can be created by replacing each non-zero entry in $\mathbf{B}$ by a sum of $B_{x,y}$ non-overlapping permutation matrices of size $M \times M$ and each zero entry by the $M \times M$ all-zero matrix. It is an important feature of this construction that each derived code inherits the degree distribution and graph neighborhood structure of the protograph. The ensemble of protograph-based LDPC-BCs with block length $n = Mn_v$ is defined by the set of matrices $\mathbf{H}$ that can be derived from a given protograph using all possible combinations of $M \times M$ permutation matrices. We denote the (J, K)-regular LDPC-BC ensemble with design rate $R = 1 - J/K$ defined by the all-ones base matrix $\mathbf{B}$ of size $J \times K$ as $\mathcal{B}_{J,K}$. The protograph representing $\mathcal{B}_{3,6}$ with $R = 1/2$ is shown in Fig. 1(a). For demonstration purposes, we also consider the protograph (shown in Fig. 1(b)) associated with the $R = 1/2$ irregular-repeat-accumulate (IRA) LDPC-BC that was specified in the WiMAX standard [21]. This irregular protograph has variable nodes with degrees ranging from 2 to 6 and check nodes with degrees 6 and 7. Puncturing of LDPC-BCs has been investigated extensively in the literature [7]-[14] and good rate-compatible protograph-based codes and code ensembles have been constructed (see, *e.g.*, [5] in the context of graph extending and [17] using puncturing).

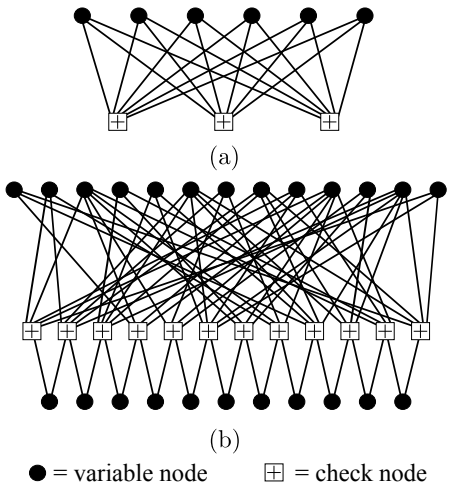

Fig. 1: Protographs associated with (a) the $(3, 6)$-regular LDPC-BC ensemble $\mathcal{B}_{3,6}$ and (b) the WiMAX IRA LDPC-BC ensemble.

B. Protograph-based SC-LDPC Codes

SC-LDPC codes are constructed by *coupling* together a series of L disjoint, or uncoupled, Tanner graphs into a single coupled chain, and they can be viewed as a type of LDPC convolutional code (LDPC-CC) [22], since spatial coupling is equivalent to introducing memory into the encoding process. SC-LDPC codes have been shown to combine excellent iterative decoding thresholds [23], [24], [18] and good asymptotic minimum distance and trapping set properties [18], [25], [26]. Moreover, it has been proven analytically for general memoryless binary-input symmetric-output (MBS) channels that the BP decoding thresholds of a class of (J, K)-regular SC-LDPC code ensembles achieve the MAP decoding thresholds of the underlying (J, K)-regular LDPC block code ensembles as $L \to \infty$, a phenomenon termed *threshold saturation* [24]. Rate-compatible LDPC-CCs were shown to be capable of achieving the capacity of the BEC using graph extending in [6]. An algorithm to select particular puncturing patterns to construct robust rate-compatible LDPC-CCs was presented in [27].

The base matrix of an SC-LDPC code ensemble with

Ensemble	Component base matrices
$\mathcal{C}_{3,4}(L)$	$\mathbf{B}_0 = \begin{bmatrix} 1 & 1 & 0 & 0 \\ 0 & 1 & 1 & 0 \\ 0 & 0 & 1 & 1 \end{bmatrix}, \mathbf{B}_1 = \begin{bmatrix} 0 & 0 & 1 & 1 \\ 1 & 0 & 0 & 1 \\ 1 & 1 & 0 & 0 \end{bmatrix}$
$\mathcal{C}_{3,6}(L)$	$\mathbf{B}_0 = \begin{bmatrix} 2 & 1 \end{bmatrix}, \mathbf{B}_1 = \begin{bmatrix} 1 & 2 \end{bmatrix}$
$\mathcal{C}_{3,6,B}(L)$	$\mathbf{B}_0 = \mathbf{B}_1 = \mathbf{B}_2 = \begin{bmatrix} 1 & 1 \end{bmatrix}$
$\mathcal{C}_{4,8}(L)$	$\mathbf{B}_0 = \mathbf{B}_1 = \begin{bmatrix} 1 & 1 \end{bmatrix}, \mathbf{B}_2 = \begin{bmatrix} 2 & 2 \end{bmatrix}$
$\mathcal{C}_{5,10}(L)$	$\mathbf{B}_0 = \begin{bmatrix} 1 & 1 \end{bmatrix}, \mathbf{B}_1 = \begin{bmatrix} 4 & 4 \end{bmatrix}$
$\mathcal{C}_{3,9}(L)$	$\mathbf{B}_0 = \begin{bmatrix} 1 & 1 & 1 \end{bmatrix}, \mathbf{B}_1 = \begin{bmatrix} 2 & 2 & 2 \end{bmatrix}$

TABLE I: SC-LDPC code ensemble component base matrices.

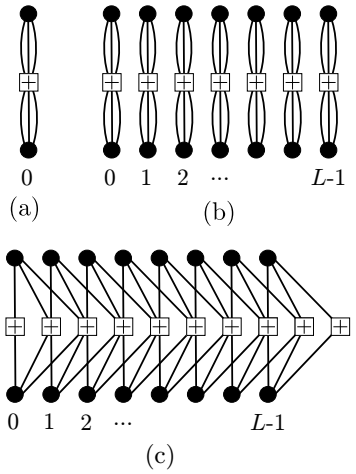

Fig. 2: Tanner graphs associated with (a) a $(3, 6)$-regular LDPC-BC protograph, (b) a chain of L uncoupled $(3, 6)$-regular LDPC-BC protographs, and (c) a chain of L spatially coupled $(3, 6)$-regular LDPC-BC protographs with coupling width $w = 2$.

coupling length L is

$$\mathbf{B}_{[0,L-1]} = \begin{bmatrix} \mathbf{B}_0 & & & \\ \mathbf{B}_1 & \mathbf{B}_0 & \ddots & \\ \vdots & \mathbf{B}_1 & \ddots & \\ \mathbf{B}_w & \vdots & \ddots & \mathbf{B}_0 \\ & \mathbf{B}_w & & \mathbf{B}_1 \\ & & \ddots & \vdots \\ & & & \mathbf{B}_w \end{bmatrix}_{(L+w)b_c \times Lb_v}, \quad (1)$$

where w denotes the *coupling width* and the $b_c \times b_v$ *component base matrices* $\mathbf{B}_i$, $i = 0, 1, \ldots, w$, represent the edge connections from the b_v variable nodes at time t to the b_c check nodes at time $t+i$. An ensemble of SC-LDPC codes can then be formed from $\mathbf{B}_{[0,L-1]}$ using the protograph construction method described above. The design rate of the ensemble of SC-LDPC codes is

$$R_L = 1 - \frac{(L+w)b_c}{Lb_v}. \quad (2)$$

The ensembles and their component base matrices used in this paper are given in Table I. Fig. 2 illustrates the "edge-spreading" construction [18] of the protograph representing the SC-LDPC code ensemble $\mathcal{C}_{3,6,B}(L)$.

III. Thresholds of Randomly Punctured LDPC Code Ensembles on the BEC

In this section, we consider the transmission of randomly punctured LDPC codes over the BEC. After summarizing the puncturing of linear codes, we then describe the channel model, showing that the problem can be analyzed by means of two cascaded BECs or, equivalently, a single BEC with a modified erasure rate. We then determine the iterative BP decoding thresholds of punctured LDPC-BC and SC-LDPC code ensembles on the BEC.

A. Puncturing Linear Codes

A linear code is *punctured* by removing a set of p columns from its generator matrix, which has the effect of reducing the codeword length from n to $n - p$. After puncturing a linear code with *puncturing fraction* $\alpha = p/n$, the resulting transmission rate is

$$R(\alpha) = \frac{R}{1-\alpha}, \quad \alpha \in [0, 1), \quad (3)$$

where $R(0) = R$ is the rate of the mother (unpunctured) code. The dimension of the code is preserved, and therefore the target rate $R(\alpha)$ is achieved, provided no two distinct codewords differ within the p punctured symbols only. This can be achieved, for example, by restricting punctured symbols to the $n-k$ parity-check symbols of a code in systematic form. A code can be punctured randomly or according to a particular pattern. It is assumed that the receiver knows the positions of the punctured symbols, and the decoder estimates both the punctured and transmitted symbols during decoding.

B. Thresholds of Randomly Punctured LDPC Code Ensembles

Consider puncturing a length n codeword $\mathbf{v}$ for transmission over a BEC with erasure probability ϵ. We assume that a fixed fraction $\alpha = p/n$ of the code symbols are punctured, such that the transmitted codeword $\mathbf{v}^{\text{punc}}$ has length $n^{\text{punc}} = (1-\alpha) \cdot n$. After transmission, the received vector $\mathbf{r}$ will contain, on average, $\epsilon \cdot n^{\text{punc}}$ erased symbols and $(1-\epsilon) \cdot n^{\text{punc}}$ correct symbols. The receiver knows the positions of the punctured and erased symbols and proceeds to decode the overall code of length n.

For the purpose of threshold analysis, we assume that, instead of applying a particular fixed puncturing pattern to each transmitted codeword, the transmitter randomly selects a different puncturing pattern for every codeword. This selection is performed uniformly from the set of all possible length n patterns with $p = \alpha n$ punctured symbols. We refer to this approach as *Strategy 1*. For large block length n, the behavior concentrates around the average, and any fixed puncturing pattern will, with high probability, result in similar performance as Strategy 1. Consider now a different random puncturing strategy, in which each symbol in a codeword is punctured independently with probability α. In this case the number of punctured symbols is not a constant but a binomially distributed random variable with mean $n\alpha$ and variance $n\alpha(1-\alpha)$. This approach is referred to as *Strategy 2*.

Lemma 1 *Consider an arbitrary code ensemble whose BP decoding threshold can be computed by means of density evolution. Assume that Strategy 1 or 2 is applied. Then, on*

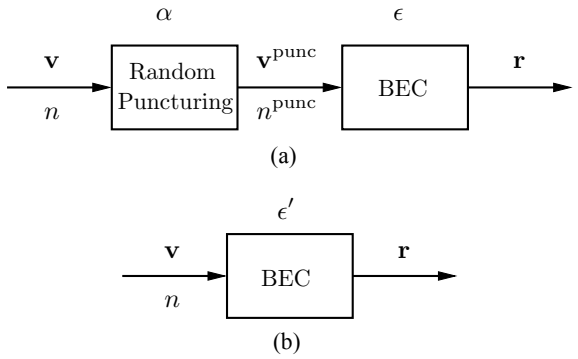

Fig. 3: (a) Block diagram illustrating random puncturing on the BEC, and (b) an equivalent BEC for random puncturing.

the BEC, the BP decoding threshold will be the same for both puncturing strategies.

Proof. In density evolution, the effect of puncturing is completely characterized by the distribution of input messages at the variable nodes. On the BEC, each message is either the correct symbol or an erasure, and thus the message distribution is determined by the probability of an erasure. An input message is erased if the corresponding received symbol is either punctured or erased by the channel, which occurs with probability $P_p + (1 - P_p)\epsilon$, where P_p denotes the probability that a symbol is punctured. For Strategy 2, each symbol is erased with probability α, which immediately implies that $P_p = \alpha$. For Strategy 1, each of the $\binom{n}{p}$ possible puncturing patterns is chosen with equal probability, and the number of patterns for which a given symbol is erased is equal to $\binom{n-1}{p-1}$. It follows that a particular symbol is erased with probability $\binom{n-1}{p-1}/\binom{n}{p} = p/n$, resulting in $P_p = \alpha$. Since both puncturing strategies result in the same distribution of input messages, their BP decoding thresholds on the BEC must be the same. □

Random puncturing using Strategy 2 can be represented as a BEC with erasure probability α. Combining this "random puncturing channel" with the actual transmission channel, as shown in Fig. 3(a), we can now model the transmission of randomly punctured codewords over the BEC as two cascaded BECs. This model is equivalent to a single BEC with crossover probability ϵ', as illustrated in Fig. 3(b), with

$$\begin{aligned}\epsilon' &= \alpha + (1-\alpha)\epsilon \\ &= 1 - (1-\epsilon)(1-\alpha)\ .\end{aligned} \tag{4}$$

Based on this model we can prove the following theorem, which according to Lemma 1 is valid for both puncturing strategies.

Theorem 2 *The BP threshold $\epsilon_{BP}(\alpha)$ of a randomly punctured LDPC code ensemble on the BEC with puncturing fraction α is given by*

$$\epsilon_{BP}(\alpha) = 1 - \frac{1-\epsilon_{BP}(0)}{R} \cdot R(\alpha), \tag{5}$$

where $\epsilon_{BP}(0) = \epsilon_{BP}$ and R are the BP threshold and design rate of the (unpunctured) mother code ensemble, respectively, and $R(\alpha)$ is the target rate after puncturing.

Proof. Consider an arbitrary code ensemble of rate R with BEC iterative BP decoding threshold ϵ_{BP}. We are interested in the threshold $\epsilon_{\text{BP}}(\alpha)$ of the punctured code ensemble with rate $R(\alpha)$. In other words, we wish to know the channel parameter $\epsilon = \epsilon_{\text{BP}}(\alpha)$ such that, after random puncturing with probability α, using Strategy 2, we obtain an equivalent channel with parameter $\epsilon' = \epsilon_{\text{BP}}(0) = \epsilon_{\text{BP}}$. Using (4), we obtain

$$\epsilon_{\text{BP}}(0) = 1 - (1 - \epsilon_{\text{BP}}(\alpha))(1-\alpha), \tag{6}$$

so that

$$\epsilon_{\text{BP}}(\alpha) = 1 - \frac{1-\epsilon_{\text{BP}}(0)}{1-\alpha}. \tag{7}$$

For Strategy 2, the expected fraction of punctured symbols is equal to α. According to Lemma 1, the same threshold is achieved with Strategy 1, for which a fixed fraction α of symbols is punctured. □

Note that (5) provides an explicit expression for the BP threshold $\epsilon_{\text{BP}}(\alpha)$ of the punctured LDPC code ensemble with puncturing fraction α as a function of the target rate $R(\alpha) \geq R$, *i.e.*, for a given puncturing fraction α, the function $\epsilon_{\text{BP}}(\alpha)$ depends only on the threshold $\epsilon_{\text{BP}}(0)$ and the rate R of the mother code ensemble. From (5), we define

$$\theta = \frac{1-\epsilon_{\text{BP}}(0)}{R} \geq 1, \tag{8}$$

where equality holds if and only if the threshold of the mother code ensemble $\epsilon_{\text{BP}}(0)$ is equal to the Shannon limit, and it follows that the largest possible rate with a non-negative threshold $\epsilon_{\text{BP}}(\alpha)$ is given by

$$R_{\max} = R(\alpha = \epsilon_{\text{BP}}(0)) = \frac{1}{\theta}\ . \tag{9}$$

Equivalently, the maximum puncturing fraction α with a non-negative BP threshold is equal to the threshold $\epsilon_{\text{BP}}(0) = \epsilon_{\text{BP}}$ of the mother code. We refer to the range of rates $R(0) \leq R(\alpha) \leq R_{\max}$ where the punctured code ensembles have non-negative thresholds as the *achievable rate range*. (The value $R_{\max}$ was referred to as the "cutoff rate" in [9].)

Note the implications of (5) and (8): *θ determines the gap to capacity for all punctured code ensembles*. This leads to the following Corollary of Theorem 2.

Corollary 3 *For BP decoding on the BEC, the gap to capacity $\Delta_{Sh}(\alpha)$ of a randomly punctured LDPC code ensemble with puncturing fraction α and a given achievable target rate $R(\alpha)$ is*

$$\begin{aligned}\Delta_{Sh}(\alpha) &= \epsilon_{Sh}(R(\alpha)) - \epsilon_{BP}(\alpha) \\ &= (\theta - 1)R(\alpha),\end{aligned} \tag{10}$$

where $\epsilon_{Sh}(R(\alpha)) = 1 - R(\alpha)$ is the Shannon limit for the randomly punctured ensemble with rate $R(\alpha)$.

A large value of θ implies that the mother code ensemble has a threshold relatively far from the Shannon limit and the gap to capacity will grow quickly with increasing α; on the

α	$R(\alpha)$	$\epsilon_{\text{BP}}(\alpha)$	$\Delta_{\text{Sh}}(\alpha)$
0	1/4	0.6474	0.1026
0.25	1/3	0.5299	0.1368
0.5	1/2	0.2948	0.2052
0.625	2/3	0.0598	0.2735

TABLE II: Thresholds and corresponding gaps to capacity for randomly punctured $(3, 4)$-regular LDPC-BC ensembles $\mathcal{B}_{3,4}$.

other hand, for a value of θ close to 1, the mother code ensemble has a threshold close to the Shannon limit and the gap to capacity will grow slowly with increasing α. In the extreme case where $\theta = 1$, *i.e.*, the threshold of the mother code ensemble is equal to the Shannon limit, then capacity is achieved for all punctured code ensembles with target rates $R(\alpha) \geq R$.

C. Numerical Threshold Results

In this section, we calculate and compare values of θ for different LDPC-BC and SC-LDPC code ensembles.

Example 1 The $\mathcal{B}_{3,4}$ LDPC-BC ensemble has BP threshold $\epsilon_{\text{BP}}(0) = 0.647$ and design rate $R(0) = 0.25$, which results in $\theta = 1.4103$. Since $\epsilon_{\text{BP}}(0) = 0.6474$ is relatively far from capacity ($\epsilon_{\text{Sh}} = 0.75$), this ensemble has a large value of θ, and consequently the gap to capacity increases significantly with increasing puncturing fraction α. Table II displays some punctured thresholds $\epsilon_{\text{BP}}(\alpha)$ with corresponding gaps to capacity $\Delta_{\text{Sh}}(\alpha)$ obtained using (5) and (10), respectively. For this ensemble, we obtain $R_{\text{max}} = 0.709$ using (9). □

Fig. 4 shows numerically calculated BP thresholds of the randomly punctured LDPC-BC ensembles $\mathcal{B}_{3,9}^{\text{punc}}(\alpha)$, $\mathcal{B}_{\text{IRA}}^{\text{punc}}(\alpha)$, $\mathcal{B}_{3,6}^{\text{punc}}(\alpha)$, $\mathcal{B}_{4,8}^{\text{punc}}(\alpha)$, $\mathcal{B}_{5,10}^{\text{punc}}(\alpha)$, and $\mathcal{B}_{3,4}^{\text{punc}}(\alpha)$ for a variety of puncturing fractions α (dots, triangles, squares, rhombuses, and crosses), along with the thresholds obtained using (5) (solid lines). The corresponding values of θ are given in Table III. The numerically calculated thresholds match (5) exactly. From $\epsilon_{\text{BP}}(\alpha) = 1 - \theta \cdot R(\alpha)$, we see that θ can be interpreted graphically as the slope of the parametrically defined line determining the positions of the punctured thresholds $\epsilon_{\text{BP}}(\alpha)$ for all α. Comparing the four rate $R = 1/2$ mother code ensembles, we find that the thresholds from best to worst are $\mathcal{B}_{\text{IRA}}^{\text{punc}}(0)$, $\mathcal{B}_{3,6}^{\text{punc}}(0)$, $\mathcal{B}_{4,8}^{\text{punc}}(0)$, $\mathcal{B}_{5,10}^{\text{punc}}(0)$. Consequently, this ordering holds for all higher achievable rates also, since the values of θ are increasing (see Table III). We stress that the gap to capacity for a given target rate does not depend on the amount of puncturing; rather, it depends solely on the value of θ obtained for the mother code ensemble. The best value of θ is obtained for $\mathcal{B}_{3,9}$; therefore, for achievable target rates $R \geq 2/3$, the thresholds of $\mathcal{B}_{3,9}^{\text{punc}}(\alpha)$ are superior to all the $R = 1/2$ mother code ensembles considered. Note that, in general, the thresholds of (J, K)-regular LDPC-BC ensembles worsen for a given target rate with increasing graph density, since the thresholds of the mother code ensembles, and hence the corresponding values of θ, worsen.

Example 2 The $\mathcal{C}_{3,4}(L = 50)$ SC-LDPC code ensemble has BP threshold $\epsilon_{\text{BP}}(0) = 0.746$ and design rate $R(0) = 0.235$,

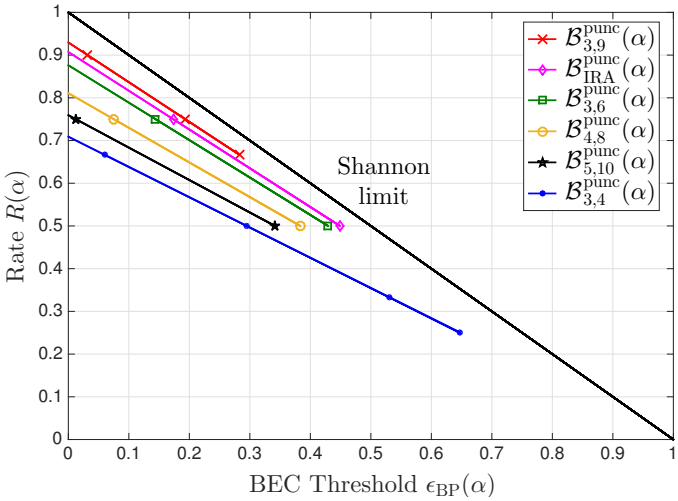

Fig. 4: BEC BP thresholds of several randomly punctured LDPC-BC code ensembles for a variety of puncturing fractions α.

			θ		
Ensemble	θ	Ensemble	$L = 20$	$L = 50$	$L = \infty$
$\mathcal{B}_{3,4}$	1.4103	$\mathcal{C}_{3,4}(L)$	1.1954	1.0810	1.0161
$\mathcal{B}_{3,6}$	1.1411	$\mathcal{C}_{3,6}(L)$	1.0776	1.0447	1.0237
$\mathcal{B}_{4,8}$	1.2331	$\mathcal{C}_{3,6,B}(L)$	1.1372	1.0664	1.0237
$\mathcal{B}_{5,10}$	1.3169	$\mathcal{C}_{4,8}(L)$	1.1162	1.0465	1.0046
$\mathcal{B}_{3,9}$	1.0757	$\mathcal{C}_{5,10}(L)$	1.0567	1.0243	1.0038
$\mathcal{B}_{\text{IRA}}$	1.1022	$\mathcal{C}_{3,9}(L)$	1.0467	1.0309	1.0205

TABLE III: Values of θ for various mother LDPC-BC and SC-LDPC code ensembles.

which results in $\theta = 1.0809$. Similarly, the $\mathcal{C}_{3,6}(L = 50)$ SC-LDPC code ensemble has $\epsilon_{\text{BP}}(0) = 0.4881$ and $R(0) = 0.49$, which results in $\theta = 1.0447$. The underlying LDPC block code ensembles $\mathcal{B}_{3,4}$ and $\mathcal{B}_{3,6}$, with rates $R(0) = 0.25$ and $R(0) = 0.5$, have thresholds $\epsilon_{\text{BP}}(0) = 0.6474$ and $\epsilon_{\text{BP}}(0) = 0.4294$, resulting in $\theta = 1.4103$ and $\theta = 1.1411$, respectively. □

The thresholds of SC-LDPC mother code ensembles improve with L. In particular, thresholds close to capacity are obtained for large L and, as a consequence, the corresponding values of θ are close to 1, and the thresholds of the randomly punctured SC-LDPC code ensembles are close to capacity for all achievable rates $R(\alpha) \leq R_{\text{max}}$. Consistent with (10), as we increase L, the gap to capacity of the randomly punctured SC-LDPC code ensembles is monotonically decreasing (improving) since θ decreases. Table III displays values of θ obtained using (8) for various mother LDPC-BC and SC-LDPC code ensembles. Comparing the $(3, K)$-regular ensembles, we find that, for large L, the $\mathcal{C}_{3,4}(L)$ ensemble has the smallest value of θ, and consequently randomly puncturing this ensemble will result in the best thresholds, even for high rates. It is also important to note that the value of θ depends on the particular "edge spreading" used to construct the protograph. For example, the ensembles $\mathcal{C}_{3,6}(L)$ and $\mathcal{C}_{3,6,B}(L)$ are both $(3, 6)$-regular, but they were constructed using different edge spreadings, which results in different values of θ for finite values of L. These considerations give rise to the interesting

question of what is the best edge spreading and (J, K) pair that minimizes θ for a fixed J. (For further discussion and examples of randomly punctured SC-LDPC code ensembles, see [19].)

Finally, we note that, unlike (J, K)-regular LDPC-BC ensembles, increasing the graph density is known to result in SC-LDPC mother code ensembles with thresholds approaching capacity for large L, which implies that the corresponding θ values approach 1. For example, we see from Table III that the $(J, 2J)$-regular, rate $R = 1/2$, SC-LDPC code ensembles have decreasing θ values, approaching 1 for large L, as J increases, whereas the LDPC-BC ensembles $\mathcal{B}_{J,2J}$ have θ values that grow with increasing J. Consequently, to achieve thresholds close to capacity for almost all rates one can puncture a single high density, low rate (J, K)-regular SC-LDPC code ensemble with large L.

D. Remarks

- If one can find a capacity approaching or capacity achieving code ensemble then it will have a θ value close to, or equal to, 1 and it will be well suited to random puncturing as discussed above. Related statements regarding capacity achieving LDPC code ensembles on the BEC with puncturing have been made before (see *e.g.*, [9], [28]). However, we note that the threshold saturation effect of spatial coupling results in (J, K)-regular SC-LDPC code ensembles with thresholds close to capacity and θ values close to 1. Without spatial coupling, one would have to design an optimized capacity approaching block code ensemble to obtain a good value of θ, or accept a poor value of θ with a (J, K)-regular LDPC-BC ensemble.
- Designing optimized irregular mother LDPC-BC ensembles to obtain a good value of θ for a given R is likely to result in an ensemble with poor minimum distance properties. In addition to having thresholds close to capacity and correspondingly good θ values, (J, K)-regular SC-LDPC mother code ensembles are known to have linear minimum distance growth [18]. In Section V, we show that this property carries over to randomly punctured SC-LDPC code ensembles.
- The derivation of the thresholds of randomly punctured LDPC code ensembles is independent of the decoding algorithm or the structure of the mother code. To determine thresholds for all punctured ensembles of rate $R \leq R(\alpha) \leq R_{\text{max}}$, we only require the threshold and the rate of the mother code. A similar argument can be made for the threshold of MAP decoding, for example. In this case, everything follows in the same way and we obtain
$$\epsilon_{\text{MAP}}(\alpha) = 1 - \theta_{\text{MAP}} \cdot R(\alpha), \tag{11}$$
for the MAP decoding threshold of a randomly punctured ensemble with puncturing fraction α and rate $R(\alpha)$, where
$$\theta_{\text{MAP}} = \frac{1 - \epsilon_{\text{MAP}}(0)}{R} \geq 1, \tag{12}$$
$\epsilon_{\text{MAP}}(0)$ is the MAP decoding threshold of the mother code ensemble, and $R = R(0)$ is the mother code ensemble rate. Also, for the MAP decoder, $R_{\text{max}} = 1/\theta_{\text{MAP}}$. Example 3 (below) provides some MAP thresholds for the randomly punctured $(3, 6)$-regular LDPC-BC ensemble.
- Due to the threshold saturation effect, certain (J, K)-regular SC-LDPC code ensembles achieve the MAP threshold of the underlying (J, K)-regular LDPC-BC ensemble with BP decoding as $L \to \infty$ [24]. Consequently, it follows from (5) and (11) that randomly punctured SC-LDPC code ensembles under BP decoding achieve the MAP threshold of the randomly punctured underlying LDPC-BC ensemble. Moreover, as we let $J \to \infty$, the MAP threshold (for an arbitrary MBS channel) of $(J, J/R)$-regular LDPC-BC ensembles improves to the Shannon limit [29], implying that the corresponding randomly punctured SC-LDPC code ensembles are capacity achieving for all $R \leq R(\alpha) \leq 1$.

α	$R(\alpha)$	$\epsilon_{\text{MAP}}(\alpha)$	$\Delta_{\text{Sh}}(\alpha)$
0	1/2	0.4881	0.0119
0.25	2/3	0.3175	0.0158
0.375	4/5	0.1810	0.0190

TABLE IV: MAP thresholds and corresponding gaps to capacity for randomly punctured $(3, 6)$-regular LDPC-BC ensembles.

Example 3 The MAP threshold of a $(3, 6)$-regular LDPC-BC ensemble is $\epsilon_{\text{MAP}}(0) = 0.4881$, resulting in $\theta_{\text{MAP}} = 1.0238$ and $R_{\text{max}} = 0.9767$. Some MAP decoding thresholds $\epsilon_{\text{MAP}}(\alpha)$ and corresponding gaps to capacity $\Delta_{\text{Sh}}(\alpha)$ are given in Table IV. □

IV. Thresholds of Randomly Punctured LDPC Code Ensembles on the BI-AWGNC

In this section, we investigate the BP thresholds of randomly punctured LDPC code ensembles on the BI-AWGNC. We begin by calculating some numerical results for a variety of ensembles and puncturing fractions. We then provide an efficient way to accurately predict BP thresholds of randomly punctured LDPC code ensembles on the BI-AWGNC, given the BP threshold of the mother code ensemble on the BEC.

A. Numerical Results

In Fig. 5, we display numerically calculated BI-AWGNC BP thresholds of the randomly punctured LDPC-BC ensembles $\mathcal{B}_{3,6}^{\text{punc}}(\alpha)$ and SC-LDPC code ensembles $\mathcal{C}_{3,6}^{\text{punc}}(L, \alpha)$ for $L = 5, 10, 50$ and a variety of puncturing fractions α. The thresholds were obtained using discretized density evolution for the BI-AWGNC, with information bit signal-to-noise ratio E_b/N_0 and noise standard deviation $\sigma = \sqrt{N_0/2}$, and are plotted in terms of σ. We observe that random puncturing of LDPC-BC and SC-LDPC code ensembles displays robust threshold performance, in the sense that, as we increase the puncturing fraction α, the thresholds do not significantly degrade and roughly track the capacity curve. To be more precise, we observe that, if the mother code ensemble has a threshold close to capacity (*e.g.*, the $\mathcal{C}_{3,6}^{\text{punc}}(50, 0)$ ensemble), then the gap to capacity increases slowly and the thresholds

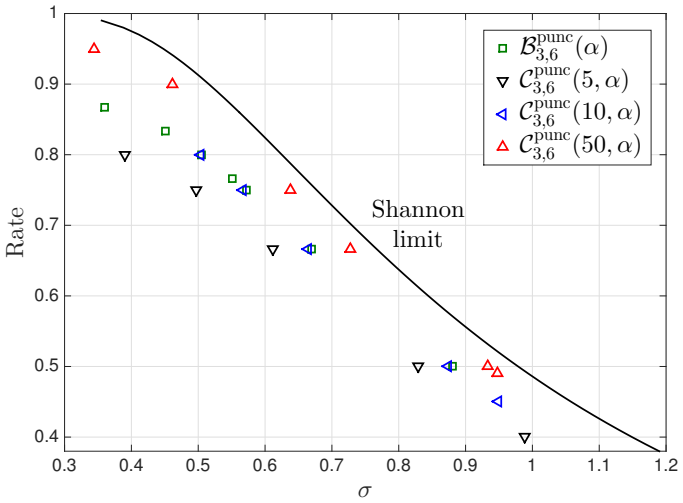

Fig. 5: Numerically calculated BI-AWGNC BP thresholds of several randomly punctured LDPC-BC and SC-LDPC code ensembles for a variety of puncturing fractions.

track the capacity curve closely as α increases. On the other hand, if the mother code ensemble has a threshold further from capacity (*e.g.*, the $\mathcal{C}_{3,6}^{\text{punc}}(5,0)$ ensemble), then the gap to capacity increases faster with increasing α.

This is analogous to the analytical result for the BEC, which follows directly from (10), where the gap to capacity of any punctured ensemble is determined by the constant θ from (8) and where the thresholds of the punctured ensembles lie on a straight line with slope determined by θ. Also, as α increases, we observe that the maximum achievable rate, *i.e.*, the maximum $R(\alpha)$ for which a BI-AWGNC BP threshold exists, is approximately equal to the value computed for the BEC using (9).

B. Predicting Thresholds

Given the similarities between the threshold results for the BEC and BI-AWGNC, a natural question arises: is it possible to predict the behavior of the thresholds of randomly punctured code ensembles on the BI-AWGNC in a similar way as for the BEC? The parameter ϵ of the BEC with uniformly distributed input X and output Y can be interpreted as the entropy

$$h_{\text{E}}(\epsilon) = H(X|Y) = 1 - C_{\text{E}}(\epsilon) = \epsilon,$$

where $C_{\text{E}}(\epsilon)$ denotes the capacity of a BEC with erasure probability ϵ. With this interpretation, (5) can be written as

$$\epsilon_{\text{BP}}(\alpha) = 1 - \theta \cdot R(\alpha) = C_{\text{E}}^{-1}(\theta \cdot R(\alpha)) = C_{\text{E}}^{-1}(f(R(\alpha))),$$

which converges to zero as $f(R(\alpha)) = \theta \cdot R(\alpha) \to 1$. The thresholds shown in Fig. 5 suggest the existence of a similar relationship for the BI-AWGNC, *i.e.*,

$$\sigma_{\text{BP}}(\alpha) = C_{\text{G}}^{-1}(f(R(\alpha))) \tag{13}$$

for some function $f(R(\alpha))$, where $C_{\text{G}}(\sigma)$ denotes the capacity of the BI-AWGNC and $\sigma_{\text{BP}}(\alpha)$ is the BP threshold in terms of the noise standard deviation σ.[1] Note that $\sigma_{\text{Sh}} = C_{\text{G}}^{-1}(R(\alpha))$ denotes the Shannon limit for a given rate $R(\alpha)$, which implies that the function $f(R(\alpha))$ characterizes the gap between the BP threshold and the Shannon limit for all achievable rates $R(\alpha) \geq R$.

In order to identify the shape of $f(R(\alpha))$, we consider the function $h_{\text{G}}(\sigma_{\text{BP}}(\alpha)) = H(X|Y) = 1 - C_{\text{G}}(\sigma_{\text{BP}}(\alpha))$. In Fig. 6, $h_{\text{G}}(\sigma_{\text{BP}}(\alpha))$ (crosses, triangles, rhombuses, circles, and squares) is plotted against the rate $R(\alpha)$ for several randomly punctured LDPC-BC and SC-LDPC code ensembles, along with the capacity $C_{\text{G}}(\sigma) = 1 - h_{\text{G}}(\sigma)$. Interestingly, we find that, as for the BEC channel, a linear relationship appears to exist between $h_{\text{G}}(\sigma_{\text{BP}}(\alpha))$ and $R(\alpha)$. Using $f(R(\alpha)) = \theta_{\text{E}} \cdot R(\alpha)$ in (13), where we now adopt the notation θ_{E} for the BEC constant θ obtained using (8), we obtain the expression

$$h_{\text{G}}(\sigma_{\text{BP}}(\alpha)) \approx 1 - \theta_{\text{E}} \cdot R(\alpha), \tag{14}$$

for $R \leq R(\alpha) \leq 1/\theta_{\text{E}}$. Predicted values of $h_{\text{G}}(\sigma_{\text{BP}}(\alpha))$ obtained using (14) are also included in Fig. 6 as solid lines. We observe that, remarkably, the approximations are almost exact, even though the value $h_{\text{G}}(\sigma_{\text{BP}}(\alpha))$ is obtained for any target rate using only θ_{E}, which just depends on the BEC threshold and rate of the mother code ensemble. For some code ensembles, we observe a slight difference in the numerically calculated values compared to the prediction, particularly for small α, as can be seen in Fig. 6. Techniques to improve the prediction even further will be discussed in Section IV-C. Finally, we note that it follows from (14) that thresholds cease to exist at precisely the same R_{max} obtained for the BEC using (9).

Now assuming $f(R(\alpha)) = \theta_{\text{E}} \cdot R(\alpha)$, we can predict BI-AWGNC thresholds in terms of noise standard deviation as

$$\sigma_{\text{BP}}(\alpha) \approx C_{\text{G}}^{-1}(\theta_{\text{E}} \cdot R(\alpha)), \tag{15}$$

for $R \leq R(\alpha) \leq 1/\theta_{\text{E}}$. Equation (15) permits a quick and easy way to approximate BI-AWGNC thresholds for any LDPC code ensemble, punctured or unpunctured, given only the BEC BP threshold and design rate. For example, the $(3,6)$-regular ensemble $\mathcal{B}_{3,6}(0)$ has $\theta_{\text{E}} = 1.1411$ and a quick calculation using (15) gives $\sigma_{\text{BP}}(0) = 0.881$, which agrees exactly with the known value [30]. Using this model, we find that the predictions are a good fit with the calculated values obtained using discretized density evolution, and that mother code ensembles with thresholds close to capacity have curves that closely track the capacity curve. (See [20] for numerical examples of both LDPC-BC and SC-LDPC code ensembles.)

Ensembles with similar values of θ_{E} will perform approximately the same for all achievable rates, even if their design rates are different. For example, the θ_{E} values for the $\mathcal{C}_{3,4}(100,0)$ and $\mathcal{C}_{3,6}(50,0)$ ensembles are 1.0475 and 1.0447, respectively. Consequently, their thresholds are approximately equal for all achievable rates $R(\alpha) \geq 1/2$. In other words, if one punctures a lower rate ensemble with a larger puncturing fraction than a higher rate ensemble in order to achieve a desired rate, there is no penalty in threshold as long as the values of θ_{E} are similar.

[1] Note that $C_{\text{E}}(x) = C_{\text{E}}^{-1}(x)$, but $C_{\text{G}}(x) \neq C_{\text{G}}^{-1}(x)$.

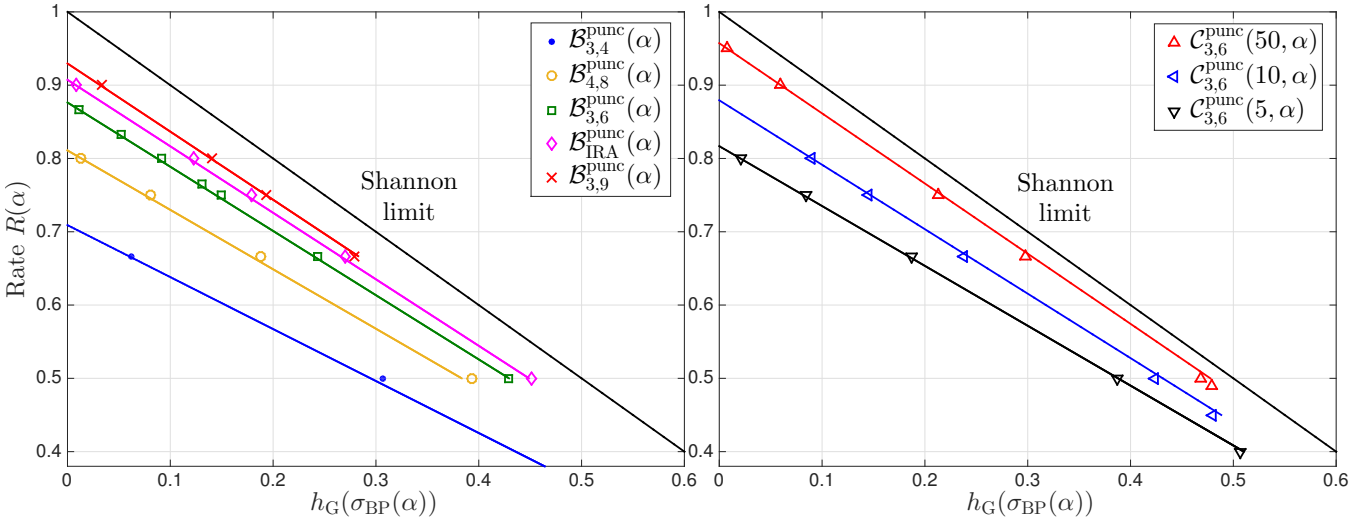

Fig. 6: Numerically calculated (markers) and predicted (solid lines) values of $h_{\mathrm{G}}(\sigma_{\mathrm{BP}}(\alpha))$ for several randomly punctured LDPC-BC (left) and SC-LDPC code ensembles (right) and a variety of puncturing fractions.

C. Improving the Prediction

In Section IV-B, it was shown that, for some ensembles, the predicted thresholds obtained using θ_{E} are less accurate for small α than for large α. This difference could be a weakness in the prediction method and/or simply a result of the numerical inaccuracy of performing discretized density evolution on the BI-AWGNC.

To improve the prediction for small puncturing fractions α, one can obtain a θ_{G}, similar to θ_{E}, based on the BI-AWGNC BP threshold $\sigma_{\mathrm{BP}}(0)$ and design rate $R = R(0)$ of the mother code ensemble as

$$\theta_{\mathrm{G}} = \frac{1 - h_{\mathrm{G}}(\sigma_{\mathrm{BP}}(0))}{R} \geq 1. \tag{16}$$

From (8) and (16), we find that $\theta_{\mathrm{G}} \approx \theta_{\mathrm{E}}$ for most code ensembles; in this case, the predictions obtained using θ_{E} are accurate for all values of α. However, the prediction is not as accurate for some code ensembles. For example, the $\mathcal{C}_{3,6}^{\mathrm{punc}}(50, 0)$ SC-LDPC code ensemble has $\theta_{\mathrm{E}} = 1.0446$ and $\theta_{\mathrm{G}} = 1.0638$. In this case, one can form an alternative prediction using

$$h_{\mathrm{G}}(\sigma_{\mathrm{BP}}(\alpha)) \approx 1 - \theta_{\mathrm{G}} \cdot R(\alpha), \tag{17}$$

for $R \leq R(\alpha) \leq R_{\max} = 1/\theta_{\mathrm{G}}$.

Fig. 7 shows numerically calculated values of $h_{\mathrm{G}}(\sigma_{\mathrm{BP}}(\alpha))$ for the $\mathcal{C}_{3,6}^{\mathrm{punc}}(50, \alpha)$ SC-LDPC code ensembles for several puncturing fractions α. Also shown are the predicted thresholds using both (14) and (17). We observe that the prediction is good for small values of α using (17) and good for large values of α using (14). Intuitively, this makes sense, since an BI-AWGNC combined with a large puncturing fraction has characteristics similar to a BEC. Moreover, we see that the calculated thresholds lie between the two predictions and a linear relationship appears to exist. Based on this observation, we can predict BI-AWGNC BP thresholds using

$$h_{\mathrm{G}}(\sigma_{\mathrm{BP}}(\alpha)) \approx \frac{R_{\max} - R(\alpha)}{R_{\max} - R(0)} \cdot h_{\mathrm{G}}(\sigma_{\mathrm{BP}}(0)), \tag{18}$$

for $R \leq R(\alpha) \leq R_{\max} = 1/\theta_{\mathrm{E}}$. Note that (18) depends on the BP threshold of the mother code ensemble for both the BI-AWGNC and the BEC. The 'mixed' prediction obtained using (18) for the $\mathcal{C}_{3,6}^{\mathrm{punc}}(50, \alpha)$ SC-LDPC code ensembles is shown in Fig. 7 by a dashed line. Fig. 8 displays some numerically calculated BI-AWGNC BP thresholds in terms of E_b/N_0 for several randomly punctured LDPC-BC and SC-LDPC code ensembles (crosses, triangles, rhombuses, circles, and squares) for a variety of puncturing fractions α along with the predicted thresholds obtained using the two parameter model (18) for rates up to $R_{\max} = 1/\theta_{\mathrm{E}}$. We observe that the predictions are accurate for all rates.[2] In summary, our results indicate that the two parameter model (18) improves the prediction in the cases where the single parameter models (15) and (17) are inaccurate (for small and large α, respectively), resulting in an accurate prediction for all α. Future work will involve an investigation of the accuracy of this prediction for general LDPC-BC and SC-LDPC code ensembles.

We conclude this section by remarking that the similarity between the thresholds on different channels when the capacity is used as a parameter was discussed by Chung in his Ph.D. thesis [31], where an erasure-channel approximation is proposed that uses the thresholds of the BEC as an approximation for the thresholds of other channels (Section 6.3, Table 6.1). Our results demonstrate that the erasure-channel approximation is even more accurate with puncturing. Furthermore, by using our knowledge of both the BI-AWGNC and BEC thresholds, our estimate does not require a density evolution recursion (which is used, for example, in the Reciprocal Channel Approximation (RCA) technique [31]). Note that it is not trivial to apply the RCA method to random puncturing, which corresponds to a Gaussian mixture scenario, and for this reason we have applied discrete density evolution.

V. Minimum Distance Growth Rates of

[2] A similar figure showing the single parameter model prediction (15) was presented in [20], where the prediction was shown to be accurate for moderate to large α, but less accurate for small α in some cases.

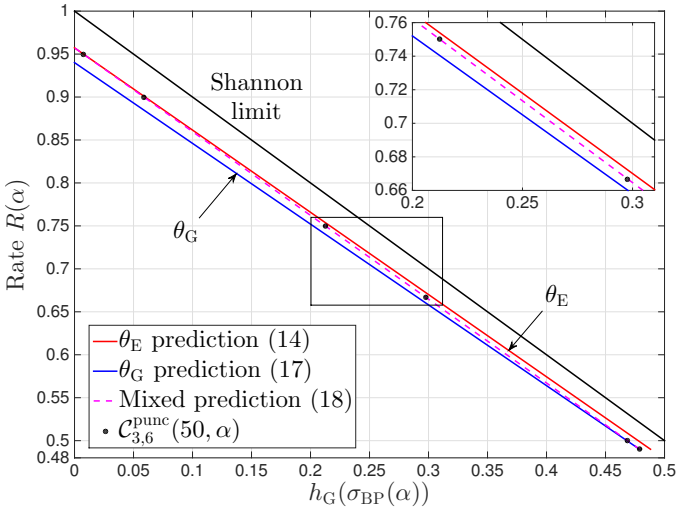

Fig. 7: Predicted BI-AWGNC BP values of $h_{\mathrm{G}}(\sigma_{\mathrm{BP}}(\alpha))$ for $\mathcal{C}_{3,6}^{\mathrm{punc}}(50,\alpha)$ SC-LDPC code ensembles.

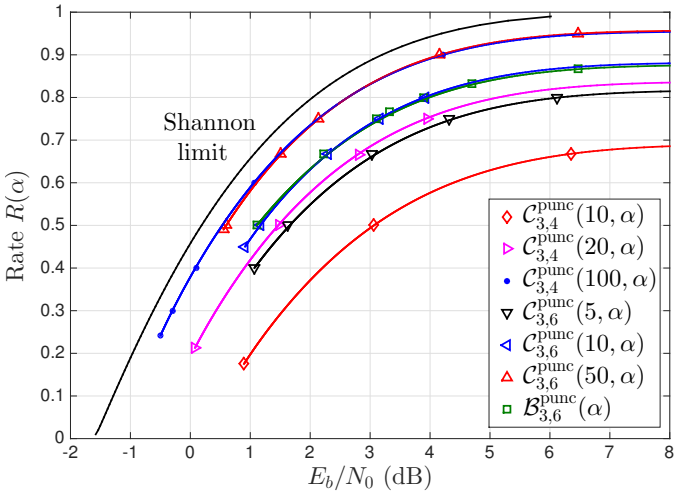

Fig. 8: Numerically calculated (markers) and predicted (solid lines) BI-AWGNC BP thresholds for several randomly punctured LDPC-BC and SC-LDPC code ensembles.

RANDOMLY PUNCTURED SC-LDPC CODE ENSEMBLES

In this section, we consider the minimum distance of randomly punctured LDPC codes. We begin by describing the asymptotic distance properties of randomly punctured code ensembles and then give numerical results for both LDPC-BC and SC-LDPC code ensembles. Although we consider protograph-based LDPC code ensembles, the results in this section are based on Theorems III.1 and IV.3 from [33] and therefore apply to any linear code ensemble.

A. Asymptotically Good Randomly Punctured LDPC Code Ensembles

For $J > 2$, (J,K)-regular LDPC-BCs are known to be *asymptotically good* [32], in the sense that the minimum distance typical of most members of the ensemble is at least as large as $\delta_{\min} \cdot n$, where $\delta_{\min} > 0$ is called the *minimum distance growth rate* of the ensemble. In [18], it was shown that ensembles of $\mathcal{C}_{J,K}(L)$ SC-LDPC codes are also asymptotically good. In this section, we investigate the distance properties of randomly punctured LDPC-BC and SC-LDPC code ensembles. (We restrict our discussion of SC-LDPC code ensembles to $\mathcal{C}_{3,6,B}^{\mathrm{punc}}(L,\alpha)$ ensembles; however, similar behavior is observed for other J and K values.)

We define the *asymptotic spectral shape* of a code ensemble as

$$r(\delta) = \limsup_{n\to\infty} \frac{1}{n} \ln(A_{\lfloor \delta n \rfloor}), \tag{19}$$

where $\delta = d/n$ is the normalized Hamming distance, $n \in \mathbb{N}$ is the block length, and A_d is the ensemble weight enumerator. The asymptotic spectral shape can be used to test if an ensemble is asymptotically good. A technique to calculate $r(\delta)$ for protograph-based block LDPC code ensembles was presented in [17]. Given the asymptotic spectral shape $r(\delta)$ of an asymptotically good code ensemble, the expected asymptotic spectral shape of the randomly punctured code ensemble can be obtained as [33]

$$r^{\mathrm{punc}}(\delta) = \frac{1}{1-\alpha}\left(\max_{0\le\lambda\le 1}\left\{\lambda \cdot h\left(\frac{(1-\alpha)\delta}{\lambda}\right) + (1-\lambda)\cdot h\left(\frac{\alpha+(1-\alpha)\delta-\lambda}{1-\lambda}\right) + r(\lambda)\right\} - h(\alpha)\right), \tag{20}$$

where $\alpha = p/n$ is the fraction of punctured bits, $0 \le \alpha < \delta_{\min}$, and $h(\delta) = -(1-\delta)\ln(1-\delta) - \delta\ln(\delta)$ is the binary entropy function. The average weight enumerators used in the formulation of (20) are obtained over all possible p-bit puncturing patterns; therefore, we require $\alpha < \delta_{\min}$ to guarantee no rate loss. For $\alpha \ge \delta_{\min}$ the rate of the ensemble can be written as $(R-\Delta_R)/(1-\alpha)$, where $\Delta_R \ge 0$. Bounds on Δ_R and conditions such that $\Delta_R = 0$ were given for (J,K)-regular LDPC-BC ensembles in [34].

B. Numerical Results

In this section, we present numerical results obtained using (20), but we do not require $\alpha < \delta_{\min}$. Consequently, there can be some rate loss with random puncturing for $\alpha \ge \delta_{\min}$, and the true rate is bounded above by $R(\alpha)$, obtained using (3). In such cases, the rates will be marked by an asterisk, or highlighted in figures with a dashed line. We note, however, that in practice the bits to be punctured would be selected to avoid rate loss by preserving the dimension of the code (semi-randomly or otherwise), and therefore the numerical results obtained in this paper are useful indicators of actual punctured code performance.

Example 4 The $(3,4)$-regular LDPC-BC ensemble $\mathcal{B}_{3,4}$ has minimum distance growth rate $\delta_{\min}(0) = 0.112$ and design rate $R(0) = 0.25$. (Recall from Section III-C that the relatively large value of $\theta = 1.4103$ in this case results in thresholds with rapidly growing gaps to capacity as α increases.) Following the technique described above, we find that the $\mathcal{B}_{3,4}^{\mathrm{punc}}(\alpha)$ code ensembles are also asymptotically good and have good minimum distance growth rates $\delta_{\min}(\alpha)$. Table V displays the growth rates $\delta_{\min}(\alpha)$ for select values of α along with the corresponding gap to the Gilbert-Varshamov (GV) bound

α	$R(\alpha)$	$\delta_{\min}(\alpha)$	$\Delta_{\text{GV}}(\alpha)$
0	$1/4$	0.1121	0.1024
0.1	$5/18$	0.1093	0.0909
0.25	$1/3^*$	0.1034	0.0706
0.5	$1/2^*$	0.0805	0.0295

TABLE V: Minimum distance growth rates and corresponding gaps to the GV bound for the randomly punctured LDPC-BC ensemble $\mathcal{B}_{3,4}$.

$\Delta_{\text{GV}}(\alpha) = \delta_{\text{GV}}(R(\alpha)) - \delta_{\min}(\alpha)$, where $\delta_{\text{GV}}(R(\alpha))$ is the GV bound for code ensembles of rate $R(\alpha)$. Note that as α increases, the design rate $R(\alpha) = 0.25/(1-\alpha)$ increases and the minimum distance growth rate decreases.[3] Also note the robust distance properties with increasing α, in the sense that $\delta_{\min}(\alpha)$ decreases slowly, resulting in decreasing gaps to the GV bound $\Delta_{\text{GV}}(\alpha)$. □

Randomly punctured SC-LDPC code ensembles display similar distance growth behavior.

Example 5 We now consider the $\mathcal{C}^{\text{punc}}_{3,6,B}(L=8,\alpha)$ ensembles. The mother code ensemble $\mathcal{C}^{\text{punc}}_{3,6,B}(8,0)$ has rate $R(0) = 0.375$ and minimum distance growth rate $\delta_{\min}(0) = 0.0324$. We find that the $\mathcal{C}^{\text{punc}}_{3,6,B}(8,\alpha)$ code ensembles are asymptotically good and have good minimum distance growth rates $\delta_{\min}(\alpha)$ for the values of α considered. (The asymptotic spectral shapes for these ensembles were drawn in [19].) We find moderate losses in minimum distance growth rate for the selected range of α (both the rate increase and distance growth rate decrease are superlinear in α). For example, puncturing 1% of the variable nodes results in a minimum distance growth rate decrease of 0.3% and puncturing 25% results in a decrease of 9.5%, while the rates increase by 0.8% and 33.3%, respectively. Regarding the latter point, we note that the resulting design rate is $R(\alpha = 0.25) = 0.5^*$ and the minimum distance growth rate $\delta_{\min}(\alpha = 0.25) = 0.029$ is larger than that of the unpunctured (equal rate) underlying $(3,6)$-regular LDPC block code ensemble, $\delta_{\min}(0) = 0.023$. Again, we find that the gap to the GV bound $\Delta_{\text{GV}}(\alpha)$ decreases with increasing α. □

Fig. 9 shows the minimum distance growth rates for randomly punctured $\mathcal{B}^{\text{punc}}_{3,4}(\alpha)$, $\mathcal{B}^{\text{punc}}_{3,6}(\alpha)$, and $\mathcal{B}^{\text{punc}}_{4,8}(\alpha)$ LDPC-BC ensembles and $\mathcal{C}^{\text{punc}}_{3,6,B}(L,\alpha)$ SC-LDPC code ensembles for $L = 3, 4, 5, 6, 7, 8, 10, 12, 14$ and a variety of puncturing fractions α. Each randomly punctured ensemble displays the same general behavior described above: the design rate increases and the minimum distance growth rates and corresponding gaps to the GV bound decrease with increasing α. (Note that the $\mathcal{B}_{\text{IRA}}(\alpha)$ ensemble is not asymptotically good, so we do not consider it in this section.) We see that the $\mathcal{B}^{\text{punc}}_{4,8}(\alpha)$ ensembles have significantly larger growth rates than the $\mathcal{B}^{\text{punc}}_{3,6}(\alpha)$ ensembles; indeed, the $\mathcal{B}^{\text{punc}}_{4,8}(\alpha)$ distance growth rates are close to the GV bound for large values of α. However, recall that the $\mathcal{B}_{4,8}(\alpha)$ ensemble has a significantly worse value of θ than the $\mathcal{B}_{3,6}(\alpha)$ ensemble, and thus the $\mathcal{B}_{4,8}(\alpha)$ ensemble thresholds are always worse (with increasing gaps to capacity as α increases). This trade-off becomes more extreme as the graph density is further increased for punctured (J,K)-regular LDPC-BC ensembles.

On the other hand, SC-LDPC code ensembles have improving values of θ (improving thresholds) for increasing L and thus provide a significant amount of flexibility for the code designer. By varying L and α, for a single code design, a large variety of rates is achievable with varying minimum distance growth rates and thresholds. The trade-offs observed for the mother SC-LDPC code ensembles in [18] are also evident for randomly punctured ensembles: θ improves with increasing L (indicating better thresholds for all achievable rates), whereas the minimum distance growth rates decrease for any fixed α with increasing L.[4]

Due to the computational complexity of evaluating the asymptotic spectral shape of SC-LDPC code ensemble protographs with large L, we have only presented numerical results for small L. However, we expect the trend in behavior observed for the values of L considered above to continue for large L: as the puncturing fraction α increases, the minimum distance growth rates $\delta_{\min}(\alpha)$ decrease from $\delta_{\min}(0)$ and the ensemble design rates $R(\alpha)$ increase from $R(0)$. Note that, for large values of L, such as those considered in Section III, the gap to capacity of the mother code is decreasing and θ is improving. We expect that, for a given large L in Fig. 9, the minimum distance growth rates $\delta_{\min}(\alpha)$ of $\mathcal{C}^{\text{punc}}_{3,6,B}(L,\alpha)$ can be approximated by a straight line originating from $\delta_{\min}(0)$, with steeper (negative) slopes as L increases (where, for a given $R(\alpha)$, $\delta_{\min}(\alpha)$ decreases as L increases).

To summarize, for sufficiently large L, SC-LDPC code ensembles have a small value of θ, resulting in thresholds close to capacity for all achievable rates; in addition, the ensembles are asymptotically good with decreasing gaps to the GV bound for increasing α. Unlike LDPC-BCs, increasing the graph density improves *both* of these measures: the thresholds approach capacity and the distance growth rates approach the GV bound.

VI. Finite Length Performance of Randomly Punctured LDPC Code Ensembles

In this section, we present BEC and BI-AWGNC computer simulations of the finite length performance of randomly punctured LDPC-BC and SC-LDPC code ensembles. All the codes simulated in this section were randomly drawn from the code ensemble according to the specified protographs and the puncturing patterns were randomized for each transmission.[5]

[3] If the puncturing fraction α is increased beyond a certain critical value greater than or equal to $\delta_{\min}$, the asymptotic spectral shape is no longer smooth. This observation is consistent with the emergence of "hook-like loops" in the spectral shapes of randomly punctured (J,K)-regular LDPC-BC ensembles for large α [33].

[4] It was noted in [18] that, due to their convolutional structure, the free distance growth rate δ_{free} of (unterminated) SC-LDPC code ensembles, which is independent of L, is a more appropriate measure of their strength than the minimum distance growth rates $\delta^{(L)}_{\min}$. Moreover, since (J,K)-regular SC-LDPC code ensembles have large δ_{free} [26], large values of α can be selected before any rate loss can occur.

[5] For practical implementation, the receiver also needs access to the puncturing pattern for successful initialization of the decoding algorithm. This could be achieved, for example, by either transmitting the puncturing pattern in the packet header, or by letting the transmitter and receiver agree on a set of random seeds before transmission begins.

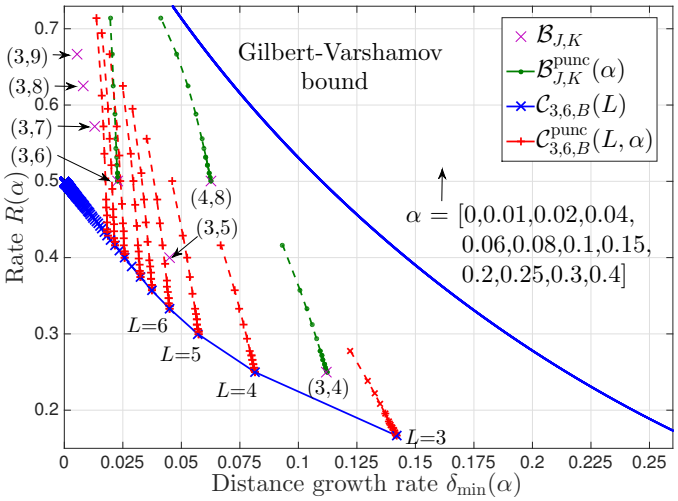

Fig. 9: Minimum distance growth rates for randomly punctured LDPC-BC and SC-LDPC code ensembles with a variety of puncturing fractions. Also shown for comparison are the minimum distance growth rates of several (J, K)-regular LDPC-BC ensembles and the GV bound.

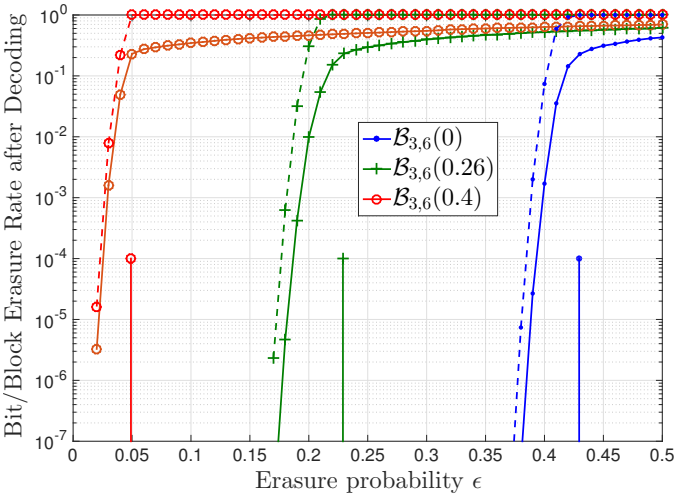

Fig. 10: BEC decoding performance and BP decoding thresholds of $(3, 6)$-regular randomly punctured LDPC-BC codes. Solid and dashed lines represent bit erasure and block erasure rates, respectively.

A. BEC Simulations

The performance of randomly punctured LDPC-BCs and SC-LDPC codes transmitted over the BEC was investigated via computer simulation. LDPC-BC examples were drawn from the $\mathcal{B}^{\text{punc}}_{3,6}(\alpha)$ ensemble with lifting factors $M = 1000$ and $M = 250$, respectively, resulting in an overall block length (decoding latency) for the unpunctured code of $n = 6000$. Puncturing fractions $\alpha = 0, 0.26$, and 0.4 were chosen, resulting in design rates $R(0) = 0.5$, $R(0.26) = 0.6757$, and $R(0.4) = 0.8333$, respectively. The performance of these codes was obtained using a standard BP decoder with a flooding update schedule and a maximum of $I_{\text{max}} = 100$ iterations. The results for these codes, shown in terms of bit erasure rate (solid lines) and block erasure rate (dashed lines), are presented in Fig. 10.

The code performance is consistent with our asymptotic code ensemble analysis. In particular, the codes display robust decoding performance, both in terms of bit and block erasure rate, with each code displaying a gap to its respective iterative decoding threshold of approximately 0.04 to 0.05 at a bit erasure rate of 10^{-5}. We expect this gap to decrease as M is increased. (This robust performance is also consistent with the finite-length scaling results of punctured LDPC codes presented in [13].) Moreover, these codes, drawn from an asymptotically good LDPC code ensemble, do not display an error floor down to a bit erasure rate of 10^{-7}. (Results for the other block code ensembles considered in this paper display similar characteristics.)

LDPC codes typically display a trade-off between waterfall and error-floor performance. For example, (J, K)-regular LDPC codes are asymptotically good for $J > 2$; however, the iterative decoding behavior of regular codes in the waterfall region of the performance curve falls short of capacity, making them unsuitable for severely power-constrained applications. On the other hand, optimized irregular LDPC codes exhibit capacity approaching performance in the waterfall but, unlike (J, K)-regular codes, are normally subject to an error floor as a result of a large number of degree two variable nodes; this makes such codes undesirable for applications that require very low decoded erasure rates. Our results confirm similar trade-offs for punctured LDPC codes, since the asymptotic properties of the punctured codes follow from those of the mother code ensemble. To the best of our knowledge, asymptotically good code ensembles do not have error floor problems for moderate code lengths (see, *e.g.*, Fig. 10). However, this is not a necessary condition, since many codes with sublinear minimum distance can have acceptably low error floors, depending on the desired application and required erasure rate.

In the case of randomly punctured SC-LDPC codes transmitted over the BEC, a mother code with code length $n = 50,000$ was drawn from the ensemble $\mathcal{C}_{3,6}(L = 50)$ with protograph lifting factor $M = 500$. This code has rate $R(0) = 0.49$. The code rate was increased by randomly puncturing 130, 200, and 220 out of every 500 variable nodes ($\alpha = 0.26, 0.4$, and 0.44, respectively), yielding code rates of $R(0.26) = 0.6622$, $R(0.4) = 0.8167$, and $R(0.44) = 0.8750$, respectively. The performance of these codes was obtained using a sliding window decoder (WD) [23], [35] with window size $W = 6$ (corresponding to a decoding latency of $2WM = 6000$ bits for the unpunctured code) and performing a maximum of $I_{\text{max}} = 10$ and $I_{\text{max}} = 20$ iterations in each window position. The results for these codes are presented in Fig. 11.

We observe robust decoding performance from the punctured SC-LDPC codes of varying rates, with each code displaying a gap to its respective iterative decoding threshold of approximately 0.05 to 0.07 at a bit erasure rate of 10^{-5}, for only a moderate lifting factor $M = 500$ and a resulting decoding latency of $2WM = 6000$ bits. We expect this gap to decrease as the lifting factor M is increased. Moreover, recall from Table III that, since $\theta = 1.0447$, the gap to capacity for the punctured thresholds is small and increases slowly as α, and thus the rate $R(\alpha)$, increases. We note from Fig. 11 that the gap between the simulated decoding performance and the

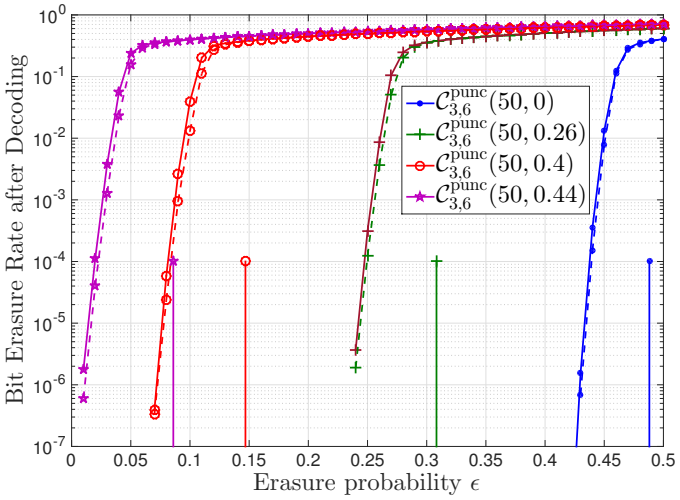

Fig. 11: BEC decoding performance and BP decoding thresholds of randomly punctured SC-LDPC codes. Solid lines represent results obtained with $I_{\text{max}} = 10$ and dashed lines represent results obtained with $I_{\text{max}} = 20$.

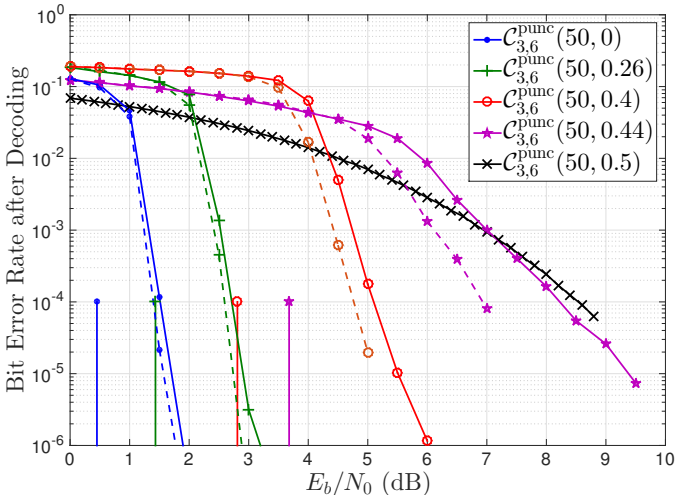

Fig. 12: BI-AWGNC decoding performance and predicted BP decoding thresholds of randomly punctured SC-LDPC codes. Solid lines represent results obtained with $I_{\text{max}} = 10$ and dashed lines represent results obtained with $I_{\text{max}} = 20$.

corresponding threshold also increases slowly as α increases and that the performance does not improve significantly by increasing the number of iterations per window position from $I_{\text{max}} = 10$ to $I_{\text{max}} = 20$, indicating $I_{\text{max}} = 10$ is sufficient to obtain the best decoding performance. We also note that, like the asymptotically good $(3, 6)$-regular LDPC-BC ensemble, we do not see any indication of an error-floor down to a bit erasure rate of 10^{-7} for codes drawn from these asymptotically good code ensembles. Comparing Figs. 10 and 11, we observe that, by using a WD, the randomly punctured SC-LDPC codes outperform the LDPC-BCs under an equal decoding latency constraint, although there is a slight code rate difference in the two cases. This is consistent with results obtained for unpunctured code ensembles [36], [37].

B. BI-AWGNC Simulations

The bit error rate (BER) performance of randomly punctured SC-LDPC codes transmitted over the BI-AWGNC was also investigated via computer simulation. The same code drawn from the $\mathcal{C}_{3,6}(50)$ ensemble and puncturing fractions that were used in Section VI-A were selected for the simulations and a sliding window decoder with $W = 6$ (corresponding to a decoding latency of $2WM = 6000$ bits) was implemented, where a maximum of $I_{\text{max}} = 10$ and $I_{\text{max}} = 20$ iterations were allowed in each window position. The results for these codes are presented in Fig. 12 along with the predicted BP thresholds obtained using (13) with $\theta_{\text{E}} = 1.0446$.

Similar to the BEC, we observe robust decoding performance from the punctured codes of varying rates. We note that the gap between the simulated decoding performance and the corresponding predicted threshold increases as the puncturing fraction α increases. For example, when α is moderate, *e.g.*, $\alpha = 0$ or 0.26, each code displays a gap to its respective predicted iterative decoding threshold of approximately 1 to 1.3dB at a BER of 10^{-5}, whereas for $\alpha = 0.4$ the gap increases to about 2dB. This should be expected for a finite length protograph-based code with a small lifting factor M; however, these gaps will decrease as M increases.

Since the capacity and threshold prediction curves are not linear (see, *e.g.*, Fig. 8), the closer we get to the maximum rate R_{max}, the more significant the gap to capacity, *i.e.*, we observe that the slope of the threshold curve flattens out (tracking the capacity curve) for higher rate punctured ensembles. It follows that, as the target rate increases beyond a certain point, the thresholds significantly degrade and the corresponding simulated performance becomes much worse. Moreover, as the puncturing fraction α becomes too large (in this case $\alpha > 0.4776$, corresponding to $R(\alpha) > R_{\text{max}} = 1/\theta_{\text{E}} = 0.938$), the threshold no longer exists and we do not observe the typical waterfall performance in the BER curve associated with codes operating below their threshold (see, *e.g.*, the black curve in Fig. 12, where $R(0.5) = 0.98$).[6] Recall that ensembles with poor θ_{E} values are characterized by a smaller maximum rate R_{max}. For example, the $\mathcal{B}_{3,6}$ ensemble has a threshold only up to $R_{\text{max}} = 0.876$. We observe that, unlike the BEC, the performance of SC-LDPC codes on the BI-AWGNC can be improved for large α by performing more than 10 iterations per window position. This behavior occurs since more iterations of the BP algorithm are required to build up reliable values for a large of punctured bits.

VII. Concluding Remarks

In this paper, we studied random puncturing of LDPC-BC and SC-LDPC code ensembles. We derived a simple analytic expression for the iterative BP decoding threshold of a randomly punctured LDPC code on the BEC and showed that, with respect to the BP threshold, the strength and suitability of an LDPC code ensemble for random puncturing is completely

[6]Since we applied a random puncturing pattern for each frame, if α is chosen to be greater than or equal to $\delta_{\min}$ of the mother code, it may cause a rate loss in some frames. This is the reason we observe the otherwise unexpected crossover in the simulated code performance for the two highest puncturing rates.

determined by a single constant $\theta \geq 1$ that depends only on the rate and the BP decoding threshold of the mother code ensemble. We then provided an efficient way to predict BP thresholds of punctured LDPC code ensembles on the BI-AWGNC, given only the BP threshold of the mother code ensemble on the BEC and the design rate, and we showed how the prediction can be improved by also considering the BI-AWGNC threshold. We demonstrated that the predictions were accurate by comparing them with values calculated using discretized density evolution for a variety of puncturing fractions. We also performed an asymptotic minimum distance analysis and showed that, for asymptotically good LDPC-BC and SC-LDPC mother code ensembles, the randomly punctured code ensembles are also asymptotically good. Moreover, we showed that, even though the minimum distance growth rates decrease with increased puncturing fraction α, the gap to the Gilbert-Varshamov bound decreases. Finally, we presented simulation results that confirm the robust decoding performance promised by the asymptotic results.

ACKNOWLEDGEMENTS

The authors would like to thank the reviewers for their constructive comments to improve the presentation of the manuscript. In particular, the comments of Reviewer 3 regarding the formulation of the random puncturing model are especially appreciated.

REFERENCES

[1] J. Hagenauer, "Rate-compatible punctured convolutional codes (RCPC codes) and their applications," *IEEE Trans. Comm.*, vol. 36, no. 4, pp. 389–400, Apr. 1988.

[2] T. Tian and C. R. Jones, "Construction of rate-compatible LDPC codes utilizing information shortening and parity puncturing," *EURASIP J. Wirel. Commun. Netw.*, vol. 2005, no. 5, pp. 789-795, Oct. 2005.

[3] J. Li and K. R. Narayanan "Rate-compatible low-density parity-check codes for capacity-approaching ARQ scheme in packet data communications," *in Proc. Int. Conf. Commun., Internet and Inf. Tech.*, pp. 201-206, Virgin Islands, USA, Nov. 2002.

[4] M. R. Yazdani and A. H. Banihashemi, "On construction of rate-compatible low-density parity-check codes," *IEEE Trans. Commun. Letter*, vol. 8, no. 3, pp. 159-161, Mar. 2004.

[5] T. Van Nguyen, A. Nosratinia, and D. Divsalar, "The design of rate-compatible protograph LDPC codes," *IEEE Trans. Commun.*, vol. 60, no. 10, pp. 2841–2850, Oct. 2012.

[6] Z. Si, R. Thobaben, and M. Skoglund, "Rate-compatible LDPC convolutional codes achieving the capacity for the BEC," *IEEE Trans. Inf. Theory*, vol. 58, no. 6, pp. 4021-4029, June 2012.

[7] J. Ha, J. Kim, D. Klinc, and S. W. Mclaughlin, "Rate-compatible puncturing of low-density parity-check codes," *IEEE Trans. Inf. Theory*, vol. 50, no. 11, pp. 2824-2836, Nov. 2004.

[8] J. Ha, J. Kim, D. Klinc, and S. W. McLaughlin, "Rate-compatible punctured low-density parity-check codes with short block lengths," *IEEE Trans. Inf. Theory*, vol. 52, no. 2, pp. 728-738, Feb. 2006.

[9] H. Pishro-Nik and F. Fekri, "Results on punctured low-density parity-check codes and improved iterative decoding techniques," *IEEE Trans. Inf. Theory*, vol. 53, no. 2, pp. 599–614, Feb. 2007.

[10] H. Y. Park, J. W. Kang, K. S. Kim and K. C. Whang, "Efficient puncturing method for rate-compatible low-density parity-check codes," *IEEE Trans. Commun.*, vol. 6, no. 11, pp. 3914-3919, Nov. 2007.

[11] J. Kim, A. Ramamoorthy, and S. W. McLaughlin, "The design of efficiently-encodable rate-compatible LDPC codes," *IEEE Trans. Commun.*, vol. 57, no. 2, pp. 365-375, Feb. 2009.

[12] M. El-Khamy, J. Hou, and N. Bhushan, "Design of rate-compatible structured LDPC codes for hybrid ARQ applications," *IEEE J. Sel. Areas Commun.*, vol. 27, no. 6, pp. 965-973, Aug. 2009.

[13] I. Andriyanova and R. Urbanke, "Waterfall region performance of punctured LDPC codes over the BEC," *Proc. IEEE Int. Symp. Inf. Theory*, Seoul, Korea, pp. 2644-2648, July 2009.

[14] H. Saeedi, H. Pishro-Nik, and A. H. Banihashemi, "Successive maximization for systematic design of universally capacity approaching rate-compatible sequences of LDPC code ensembles over binary-input output-symmetric memoryless channels," *IEEE Trans. Commun.*, vol. 59, no. 7, pp. 1807-1819, July 2011.

[15] A. I. V. Casado, W. Weng, S. Valle, and R.D. Wesel, "Multiple-rate low-density parity-check codes with constant blocklength," *IEEE Trans. Commun.*, vol. 57, no. 1, pp. 75-83, Jan. 2009.

[16] J. Thorpe, "Low-density parity-check (LDPC) codes constructed from protographs," Jet Propulsion Laboratory, Pasadena, CA, INP Progress Report 42-154, Aug. 2003.

[17] D. Divsalar, S. Dolinar, C. Jones, and K. Andrews, "Capacity-approaching protograph codes," *IEEE J. Sel. Areas Commun.*, vol. 27, no. 6, pp. 876–888, Aug. 2009.

[18] D. G. M. Mitchell, M. Lentmaier, and D. J. Costello, Jr., "Spatially coupled LDPC codes constructed from protographs," *IEEE Trans. Inf. Theory*, vol. 61, no. 9, pp. 1-24, Sep. 2015.

[19] D. G. M. Mitchell, M. Lentmaier, A. E. Pusane, and D. J. Costello, Jr., "Randomly Punctured Spatially Coupled LDPC Codes," *Proc. Int. Symp. Turbo Codes & Iterative Inf. Processing*, Bremen, Germany, Aug. 2014, pp. 1–6.

[20] D. G. M. Mitchell, M. Lentmaier, A. E. Pusane, and D. J. Costello, Jr., "Approximating Decoding Thresholds of Punctured LDPC Code Ensembles on the AWGN Channel," *Proc. IEEE Int. Symp. Inf. Theory*, Hong Kong, China, June 2015, pp. 421–425.

[21] *Air Interface for Fixed and Mobile Broadband Wireless Access Systems IEEE P802.16e/D12*, Std., Oct. 2005.

[22] A. Jiménez Felström and K. Sh. Zigangirov, "Time-varying periodic convolutional codes with low-density parity-check matrices," *IEEE Trans. Inf. Theory*, vol. 45, no. 6, pp. 2181–2191, Sept. 1999.

[23] M. Lentmaier, A. Sridharan, D. J. Costello, Jr., and K. Sh. Zigangirov, "Iterative decoding threshold analysis for LDPC convolutional codes," *IEEE Trans. Inf. Theory*, vol. 56, no. 10, pp. 5274–5289, Oct. 2010.

[24] S. Kudekar, T. Richardson, and R. Urbanke, "Spatially coupled ensembles universally achieve capacity under belief propagation," *IEEE Trans. Inf. Theory*, vol. 59, no. 12, pp. 7761–7813, Dec. 2013.

[25] D. G. M. Mitchell, M. Lentmaier, and D. J. Costello, Jr., "AWGN channel analysis of terminated LDPC convolutional codes," in *Proc. Inf. Theory and Applications Workshop*, San Diego, CA, Feb. 2011.

[26] D. G. M. Mitchell, A. E. Pusane, and D. J. Costello, Jr., "Minimum distance and trapping set analysis of protograph-based LDPC convolutional codes," *IEEE Trans. Inf. Theory*, vol. 59, no. 1, pp. 254–281, Jan. 2013.

[27] H. Zhou, D. G. M. Mitchell, N. Goertz, and D. J. Costello, Jr., "Robust rate-compatible punctured LDPC convolutional codes," *IEEE Trans. Commun.*, vol. 61, no. 11, pp. 4428–4439, Nov. 2013.

[28] C.-H. Hsu and A. Anastasopoulos, "Capacity-achieving codes with bounded graphical complexity and maximum likelihood decoding," *IEEE Trans. Inf. Theory*, vol. 56, no. 3, pp. 992–1006, Mar. 2010.

[29] G. Miller and D. Burshtein, "Bounds on the maximum-likelihood decoding error probability of low-density parity-check codes," *IEEE Transactions on Information Theory*, vol. 47, no. 7, pp. 2696–2710, Nov. 2001.

[30] T. J. Richardson and R. L. Urbanke, *Modern coding theory*. Cambridge University Press, 2008.

[31] S.-Y. Chung, "On the construction of some capacity-approaching coding schemes," Ph.D. dissertation, Massachusetts Institute of Technology, Cambridge, MA, Sept. 2000.

[32] R. G. Gallager, "Low-density parity-check codes," Ph.D. dissertation, Massachusetts Institute of Technology, Cambridge, MA, 1963.

[33] E. C. Boyle and R. J. McEliece, "Asymptotic weight enumerators of randomly punctured, expurgated and shortened code ensembles," in *Proc. Forty-Sixth Annual Allerton Conference*, Monticello, IL, Sept. 2008.

[34] C.-H. Hsu and A. Anastasopoulos, "Capacity achieving LDPC codes through puncturing," *IEEE Trans. Inf. Theory*, vol. 54, no. 10, pp. 4698–4706, Oct. 2008.

[35] A. R. Iyengar, M. Papaleo, P. H. Siegel, J. K. Wolf, A. Vanelli-Coralli, and G. E. Corazza, "Windowed decoding of protograph-based LDPC convolutional codes over erasure channels," *IEEE Trans. Inf. Theory*, vol. 58, no. 4, pp. 2303–2320, Apr. 2012.

[36] M. Lentmaier, M. M. Prenda, and G. Fettweis, "Efficient message passing scheduling for terminated LDPC convolutional codes," in *Proc.*

IEEE Int. Symp. Inf. Theory, St. Petersburg, Russia, Aug. 2011, pp. 1826–1830.

[37] K. Huang, D. G. M. Mitchell, L. Wei, X. Ma, and D. J. Costello, Jr., "Performance comparison of LDPC block and spatially coupled codes over GF(q)," *IEEE Trans. Commun.*, vol. 63, no. 3, pp. 592–604, Mar. 2015.

David G. M. Mitchell received the Ph.D. degree in Electrical Engineering from the University of Edinburgh, United Kingdom, in 2009. He is currently an Assistant Professor in the Klipsch School of Electrical and Computer Engineering at the New Mexico State University, USA. He previously held Visiting Assistant Professor and Post-Doctoral Research Associate positions in the Department of Electrical Engineering at the University of Notre Dame, USA. His research interests are in the area of digital communications, with emphasis on error control coding and information theory.

Michael Lentmaier received the Dipl.-Ing. degree in electrical engineering from University of Ulm, Germany in 1998, and the Ph.D. degree in telecommunication theory from Lund University, Sweden in 2003. He then worked as a Post-Doctoral Research Associate at University of Notre Dame, Indiana and at University of Ulm. From 2005 to 2007 he was with the Institute of Communications and Navigation of the German Aerospace Center (DLR) in Oberpfaffenhofen, where he worked on signal processing techniques in satellite navigation receivers. From 2008 to 2012 he was a senior researcher and lecturer at the Vodafone Chair Mobile Communications Systems at TU Dresden, where he was heading the Algorithms and Coding research group. Since January 2013 he is an Associate Professor at the Department of Electrical and Information Technology at Lund University. His research interests include design and analysis of coding systems, graph based iterative algorithms and Bayesian methods applied to decoding, detection and estimation in communication systems. He is a senior member of the IEEE and served as an editor for IEEE Communications Letters from 2010 to 2013 and IEEE Transactions on Communications since 2014. He was awarded the Communications Society & Information Theory Society Joint Paper Award (2012) for his paper "Iterative Decoding Threshold Analysis for LDPC Convolutional Codes."

Ali E. Pusane received the B.Sc. and M.Sc. degrees in electronics and communications engineering from Istanbul Technical University, Istanbul, Turkey, in 1999 and 2002, respectively, and the M.Sc. degree in electrical engineering, the M.Sc. degree in applied mathematics, and the Ph.D. degree in electrical engineering from the University of Notre Dame, Notre Dame, IN, in 2004, 2006, and 2008, respectively. He was a Visiting Assistant Professor at the Department of Electrical Engineering, University of Notre Dame, during 2008-2009. He is currently an Associate Professor at the Department of Electrical and Electronics Engineering, Bogazici University, Istanbul, Turkey. His research is in coding theory and wireless communications.

Daniel J. Costello, Jr. received his Ph.D. in Electrical Engineering from the University of Notre Dame in 1969. Since 1985, he has been a Professor of Electrical Engineering at Notre Dame and from 1989 to 1998 served as Chair of the Department. In 2000, he was named the Leonard Bettex Professor of Electrical Engineering.

Dr. Costello has been a member of IEEE since 1969 and was elected Fellow in 1985. In 2000, the IEEE Information Theory Society selected him as a recipient of a Third-Millennium Medal, he was a co-recipient of the 2009 IEEE Donald G. Fink Prize Paper Award and the 2012 ComSoc & Information Theory Society Joint Paper Award, and he received the 2013 IEEE Information Theory Society Aaron D. Wyner Distinguished Service Award and the 2015 IEEE Leon J. Kirchmayer Graduate Teaching Award.

Dr. Costello's research interests are in the area of digital communications, with emphasis on error control coding and coded modulation. He has numerous technical publications in his field, and in 1983 he co-authored a textbook entitled "Error Control Coding: Fundamentals and Applications", the 2nd edition of which was published in 2004.